

# R2GenCSR: Mining Contextual and Residual Information for LLMs-based Radiology Report Generation

Xiao Wang<sup>1</sup>, Yuehang Li<sup>1</sup>, Fuling Wang<sup>1</sup>, Shiao Wang<sup>1</sup>, Chuanfu Li<sup>2</sup>, Bo Jiang<sup>1\*</sup>

<sup>1</sup> School of Computer Science and Technology, Anhui University, Hefei, China

<sup>2</sup> First Affiliated Hospital of Anhui University of Chinese Medicine, Hefei, China

xiaowang@ahu.edu.cn, e23201112@stu.ahu.edu.cn, 18870722722@163.com,

wsa1943230570@126.com, licf@ahtcm.edu.cn, zeyiabc@163.com

## Abstract

Inspired by the tremendous success of Large Language Models (LLMs), existing Radiology report generation methods attempt to leverage large models to achieve better performance. They usually adopt a Transformer to extract the visual features of a given X-ray image, and then, feed them into the LLM for text generation. How to extract more effective information for the LLMs to help them improve final results is an urgent problem that needs to be solved. Additionally, the use of visual Transformer models also brings high computational complexity. To address these issues, this paper proposes a novel context-guided efficient radiology report generation framework. Specifically, we introduce the Mamba as the vision backbone with linear complexity, and the performance obtained is comparable to that of the strong Transformer model. More importantly, we perform context retrieval from the training set for samples within each mini-batch during the training phase, utilizing both positively and negatively related samples to enhance feature representation and discriminative learning. Subsequently, we feed the vision tokens, context information, and prompt statements to invoke the LLM for generating high-quality medical reports. Extensive experiments on three X-ray report generation datasets (i.e., IU X-Ray, MIMIC-CXR, CheXpert Plus) fully validated the effectiveness of our proposed model. The source code is available at [https://github.com/Event-AHU/Medical\\_Image\\_Analysis](https://github.com/Event-AHU/Medical_Image_Analysis).

## 1. Introduction

X-ray image based radiology report generation is one of the typical applications of Artificial Intelligence (AI) in healthcare. It aims to utilize powerful AI models to directly

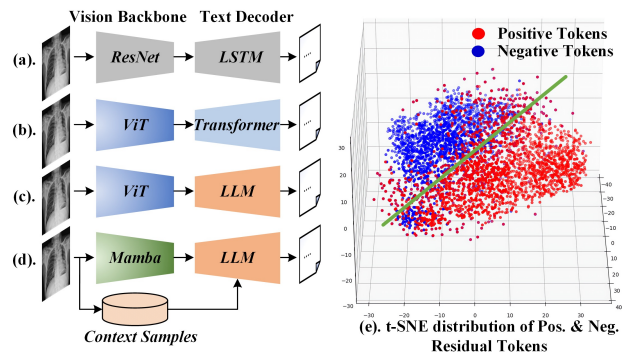


Figure 1. Comparison between (a-c). existing X-ray report generation frameworks and (d). our newly proposed one; (e). t-SNE feature distribution of our sampled positive and negative context samples from IU X-Ray dataset.

generate high-quality medical reports from given X-ray images, thereby alleviating the workload of doctors and reducing patient waiting times. Although the performance of this task has made significant strides with the development of AI, it still falls short of matching the expertise of professional physicians due to various challenges. Due to privacy concerns surrounding X-ray data, there is a lack of quality and diversity in the training datasets, and the rarity of certain diseases and abnormal conditions also results in poor generalization performance of the models. Therefore, the research on X-ray image based report generation is still a very important but unsolved problem.

Due to the good generalization of deep learning, the performance of radiology report generation has seen steady improvements. For example, Cao et al. propose the Multi-modal Memory Transformer Network (MMTN) [5] for image-report consistent radiology report generation. Jin et al. introduce the PromptMRG [21] which attempts to enhance the diagnostic accuracy in the report by feeding diagnosis-aware prompts. Li et al. proposed a new radi-

\*Corresponding Author: Bo Jiang

ological reports DCL [26] framework that uses dynamic graphs to integrate specific and general knowledge to improve visual representation. This framework also enhances visual and textual representation by leveraging contrastive learning objectives. KiUT [20] utilizes the U connection between the encoder and decoder to effectively integrate different levels of visual information. It introduces a knowledge graph and uses a distillation technique to produce reports that are more aligned with real-world conditions. ME-Transformer [55] simulates multi-expert joint diagnostics by introducing multiple learnable “expert” tokens. These tokens focus on different areas while interacting with each other to capture reliable and complementary visual information, facilitating the parallel generation of diagnostic reports. Although these models have achieved good results, their overall performance is still far from reaching the level of human experts. How to narrow the gap further with professional doctors remains a question worth pondering and researching.

Inspired by the great success of LLMs in natural language processing (NLP), some researchers also introduced LLMs for radiology report generation. Specifically, Liu et al. [28] propose to augment the LLMs-based radiology report generation using in-domain instance induction and coarse-to-fine decoding. Although better performance can be obtained, these models still achieve their efficiency and performance bottlenecks due to the following issues: **Firstly**, the performance of current LLMs heavily relies on the tokens humans feed into, for example, the prompt sentence, visual tokens, etc. More comprehensive inputs can guide the LLMs to generate high-quality medical reports. However, seldom of current works consider the context samples (e.g., the samples with/without disease) which may be very important cues for the text generation of the current sample. **Secondly**, they adopt the Transformer network as the vision backbone which is computationally expensive ( $\mathcal{O}(N^2)$ ). When handling long-range visual tokens (e.g., the raw X-ray images are usually high-definition), the self-attention in the Transformer often performs poorly on the speed, memory usage, etc.

With these issues in mind, in this work, we propose a novel radiology report generation framework that adopts the Mamba [14] as the backbone and mines the context samples to guide the large language models for high-quality report generation. A comparison between existing models and ours is illustrated in Fig. 1 (a-d). We partition the input X-ray image into patches and project them into visual tokens. Then, the Mamba backbone network is adopted for efficient and effective visual token processing. More importantly, we retrieve some context samples from the training subset for each image in the mini-batch to help our report generator understand which samples are likely to have diseases and which do not. The motivation for retrieving both posi-

tive and negative samples is to provide the LLM with contrastive contextual cues: positive cases highlight disease-related visual patterns, while negative cases serve as normal references. This contrast helps the model to better capture the subtle residual differences between abnormal and normal structures, thereby guiding the LLM to generate more accurate and clinically meaningful reports. These context samples are also processed using the Mamba backbone and subtracting the global tokens of the current image to get the residual tokens. We provide the context prompts to assist the LLM in distinguishing whether certain tokens are related to diseases. As shown in Fig. 1 (e), it is easy to find that these retrieved positive and negative samples are easily distinguishable from the perspective of the t-SNE [48] feature distribution. Finally, we feed these visual tokens, context tokens, and prompts into the LLM for high-quality radiology report generation. Extensive experiments on two widely used benchmark datasets fully validated the effectiveness of our proposed framework.

To sum up, the main contributions of this work can be listed as follows:

- 1). We propose a novel large language model based radiology report generation framework that is augmented by context samples in the training phase, termed R2GenCSR. Our approach effectively utilizes both positive and negative samples to guide the model, enhancing its ability to generate more accurate and contextually relevant reports.
- 2). We introduce a residual-guided approach for improved report generation by capturing the semantic differences between visual and textual information, providing a new perspective on combining multi-modal data (medical images and clinical texts).
- 3). Extensive experiments on the widely used IU X-Ray, MIMIC-CXR, and CheXpert Plus datasets fully validated the effectiveness of our proposed X-ray report generation framework.

## 2. Related Work

### 2.1. Radiology Report Generation

Radiology report generation (RRG), also referred to as medical report generation (MRG), focuses on generating diagnostic reports from medical images. Existing approaches can be categorized into CNN-based, RNN-based, and Transformer-based frameworks. To be specific, Li et al. [25] propose a model that combines CNNs and RNNs to generate medical reports from chest X-ray images. Jing et al. [22] propose to predict the possible diseases using LSTM [17] and then generate medical reports based on those predictions. Chen et al. [7] demonstrate the effectiveness of generating detailed and accurate radiological reports from X-ray images using the Transformer model, leveraging visual and text data to improve performance. Yang et

al. [61] addresses the visual-to-semantic gap in medical image report generation by employing a triple-branch network to jointly encode deep visual and semantic embeddings. Huang et al. [19] leverages a medical knowledge dictionary to bridge the semantic gap between visual and text modalities. Wang et al. [52] pre-train a ViT model on the high-resolution X-ray images using masked auto-encoder for radiology report generation. Zhang et al. [66] proposes a unified Med-VLP framework with multi-task paired masking with alignment module to enhance cross-modal interaction and semantic representation. Different from existing works, in this paper, we propose a novel context sample retrieval-guided LLMs framework for radiology report generation, thus, our model becomes more sensitive and accurate in predicting diseases.

## 2.2. Large Language Models

The integration of Large Language Models (LLMs) into radiology report generation has become a prominent research direction. LLMs can be categorized into two types: base LLMs and domain-specific LLMs. Early foundational models like Google’s BERT [11] and Meta’s LLaMA [46] have demonstrated significant advancements in natural language processing. OpenAI’s GPT series, particularly GPT-3 [4], has further pushed the boundaries of language generation and understanding with its 175 billion parameters.

In the medical domain, LLMs have been tailored for specific tasks. R2Gen-GPT [54] integrates image and text features into the LLaMA2-7B [47] decoder for report generation. RGRG [45] adopts a GPT-2 [40]-based approach to generate and reconnect sentences for detected regions. Google’s Med-PaLM2 [41], built on PaLM 2 [1], achieve state-of-the-art performance through domain-specific fine-tuning. MedVersa [67] extends capabilities to multimodal medical inputs and real-time task specification. Inspired by these works, we propose enhancements to radiology report generation using LLMs.

## 2.3. State Space Model

To address the high computational cost of Transformer networks, State Space Models (SSMs) [53] have been proposed to achieve linear complexity. The S4 model [15] introduces a structured state space approach, improving long-sequence dependency modeling while enhancing efficiency and accuracy. S5 [43] further simplifies and optimizes S4, balancing computational efficiency and sequence modeling capabilities. Mamba [14] advances SSMs with a time-varying state-space model and selection mechanism, enabling efficient long-sequence modeling. In vision-related tasks, SSMs have shown promising results. Vim [68] (Vision Mamba) achieves high performance and efficiency by incorporating positional embeddings and bidirectional SSMs for high-resolution image processing. VMamba [33]

introduces a Cross-Scan Module (CSM) to ensure global receptive fields with linear complexity. Mamba-2 [9] further enhances the Mamba architecture by integrating SSD theory and structural attention mechanisms.

Inspired by the linear computational cost, in this work, we propose to encode the X-ray image using a half-precision vision Mamba network and achieve similar performance on three radiology report generation benchmark datasets.

## 2.4. Context Sample Retrieving

Retrieval-Augmented Generation (RAG) is a hybrid approach that combines retrieval and generation to enhance the performance of NLP tasks, particularly those requiring extensive knowledge and contextual information. Recent advancements in retrieval-augmented methods have demonstrated their effectiveness across various domains. For instance, MedGraphRAG [56] proposes a graph-based U-Retrieval framework that combines Top-down Precise Retrieval with Bottom-up Response Refinement to balance global context awareness with fine-grained indexing. Similarly, BGFormer [51] introduces a Structure-constrained Self-attention (SSA) mechanism to mine relationships between samples for robust data representation, while CricaVPR [35] leverages cross-image differences like perspective and illumination to generate more robust image features. CRAG [60] enhances retrieval quality through a search evaluator and large-scale web searches, and EgoInstructor [57] utilizes third-person video resources to improve first-person video understanding. Additionally, RALF [18] retrieves similar layout examples to address challenges in capturing high-dimensional layout structures, and EVCAP [24] constructs external visual-name memory for retrieval-augmented image captioning. Contrastive Attention (CA) [30] leverages differences between positive and negative X-ray samples to highlight disease-specific features. In contrast, our residuals are computed in the shared embedding space of visual features and textual prompts, guiding the LLM to better distinguish disease-relevant information for more accurate report generation.

In the field of medical report generation, RAG can also serve as a clinical decision support tool by combining medical databases and research papers, helping physicians quickly access the latest research on disease diagnosis, treatment options, and drug information. Our extensive experiments on three benchmark datasets support the effectiveness of context samples for the medical report generation task.

## 3. Methodology

In this section, we will first give a review of the Mamba network and an overview of our proposed R2GenCSR framework. Then, we will dive into the details of the

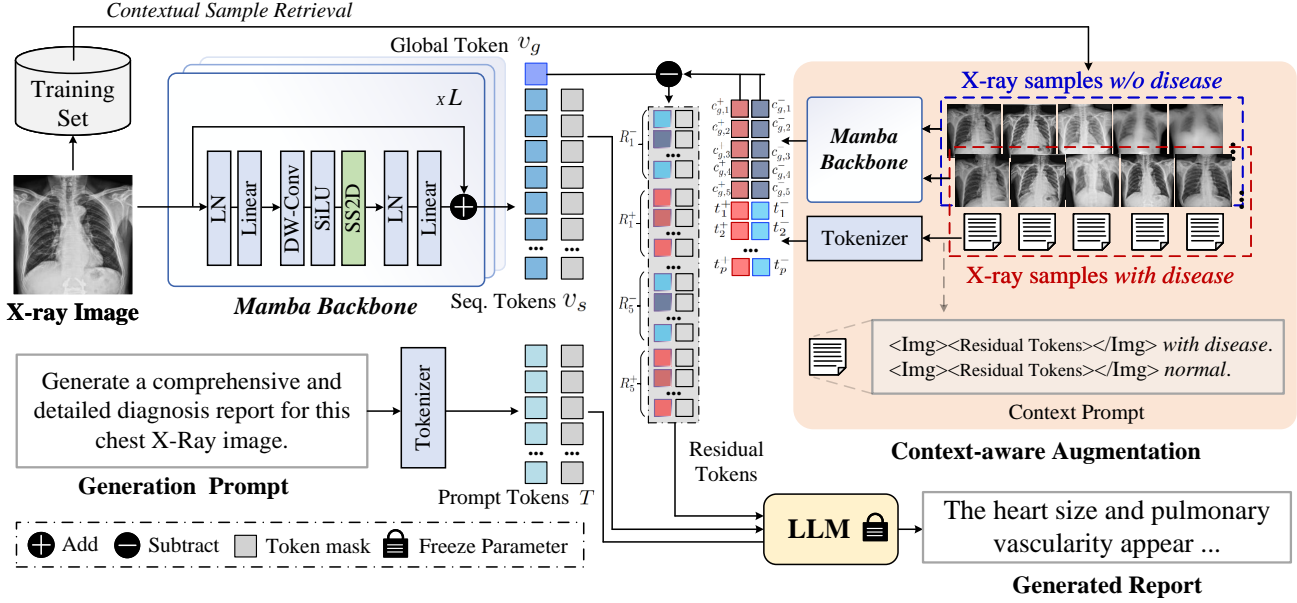


Figure 2. An overview of our proposed context sample augmented large language model for efficient radiology report generation, termed R2GenCSR. Three main modules are involved in this framework, including the Mamba vision backbone, context sample retrieval, and large language model (LLM). We first extract the visual tokens of the input X-ray image using the Mamba backbone, then, retrieve context samples from the training subset. Residual tokens are then computed by subtracting the projected context sample tokens from the projected input image tokens, all within the LLM’s text embedding space. The LLM takes the vision tokens, context residual tokens, and prompt statements as input to generate a high-quality medical report.

R2GenCSR framework, with a focus on Input Representation, Context Sample Retrieval, LLM for Report Generation, and Loss Function. More details will be introduced in the subsequent subsections.

### 3.1. Preliminary: Mamba

Current widely used Mamba networks are developed based on the continuous SSMs. It maps a one-dimensional function or sequence  $x(t) \in \mathbb{R}^p$  to  $y(t) \in \mathbb{R}^q$  through a hidden state  $h(t) \in \mathbb{R}^n$ . The computing procedure can be summarized as follows:

$$h'(t) = \mathbf{A}h(t) + \mathbf{B}x(t), \quad y(t) = \mathbf{C}h(t), \quad (1)$$

where  $\mathbf{A} \in \mathbb{R}^{n \times n}$ ,  $\mathbf{B} \in \mathbb{R}^{n \times p}$ ,  $\mathbf{C} \in \mathbb{R}^{q \times n}$  denotes the state matrix, input matrix, and output matrix.

As the image and text we processed are discrete data, the aforementioned continuous SSMs needed to be transformed into discrete ones. For example, the S4 [15] and Mamba model adopts the Zero-Order Hold (ZOH) to realize this goal, i.e.,

$$\bar{\mathbf{A}} = \exp(\Delta \mathbf{A}), \quad (2)$$

$$\bar{\mathbf{B}} = (\Delta \mathbf{A})^{-1}(\exp(\Delta \mathbf{A}) - \mathbf{I}) \cdot \Delta \mathbf{B}, \quad (3)$$

where the  $\Delta$  is a timescale parameter (also called step size).

Thus, we can reformulate the discrete version of SSMs as:

$$h_t = \bar{\mathbf{A}}h_{t-1} + \bar{\mathbf{B}}x_t, \quad y_t = \mathbf{C}h_t. \quad (4)$$

To further strengthen the SSM, Gu et al. propose the Mamba [14] which makes the model varying from time-invariant to dependent. Inspired by the success of Mamba in NLP, researchers also adapt it to the computer vision community such as VMamba [33] and Vim [68]. As shown in Eq. 4, the recursive structure offers two architectural advantages for X-ray images. First, the hidden state  $h_t$  serves as a cumulative memory of previously processed patches. When an image is flattened into patches, each new patch is integrated with the aggregated representation of all preceding patches. This creates an implicit global receptive field without the quadratic cost of explicit attention, which is clinically valuable for chest X-ray images where pathologies often manifest as spatially distributed patterns. Second, the selective mechanism in Mamba makes matrices  $\bar{\mathbf{A}}$  and  $\bar{\mathbf{B}}$  input-dependent, allowing dynamic adjustment of information retention. Patches containing abnormalities can be selectively emphasized in the state update, while normal anatomical structures can be compressed.

### 3.2. Overview

In this paper, we propose a novel contextual sample retrieval guided large language model framework for efficient

radiology report generation. As shown in Fig. 2, it can be divided into three main parts, i.e., the Mamba vision backbone, context retrieval module, and large language model (LLM) for report generation. Given the X-ray image, we first extract its visual tokens using the Mamba backbone. Meanwhile, we retrieve context samples (X-ray samples with and without disease) from the training subset based on the input image and embed them into visual and text tokens. Then, the residual tokens which measure the difference between the input and context samples can be obtained via the subtract operator. Finally, we feed the vision tokens, context residual tokens, and prompt statements into the LLM to generate a high-quality medical report. One can note that the proposed framework stands out from existing methods by *incorporating context retrieval* and *using a linear complexity vision backbone*, which enhances feature representation and discriminative learning while maintaining computational efficiency.

### 3.3. R2GenCSR Framework

In this subsection, we will introduce the R2GenCSR framework from the perspective of *Input Representation*, *Context Sample Retrieval*, *LLM for Report Generation*, and *Loss Function*.

#### 3.3.1 Input Representation

Assume the dataset contains  $N$  X-ray images,  $\mathbf{X} = \{x_1, x_2, \dots, x_N\}$ , where each  $x_i \in \mathbb{R}^{C \times H \times W}$  represents a X-ray image with  $C$  channels, height  $H$ , and width  $W$ . For each X-ray image  $x$ , the corresponding feature map  $v \in \mathbb{R}^{\hat{H} \times \hat{W} \times \hat{C}} = VMamba(x)$  can be obtained after feeding it into the VMamba backbone, where  $\hat{H}$  and  $\hat{W}$  are the spatial dimensions of the feature map, and  $\hat{C}$  is the number of feature channels. The reason our framework adopts VMamba instead of conventional visual Transformer models, such as ViT and Swin-Transformer, is because the computational complexity of this model is linear ( $\mathcal{O}(N)$ ), requiring lower computational resources. As shown in Fig. 2, the basic VMamba block consists of Layer Normalization (LN), Linear Layer, DW-Conv layer, SiLU activation layer, SS2D module, and also the skip connections.

Then, two distinct types of representations are generated based on feature map  $v$ , i.e., global features  $v_g$  and sequential tokens  $v_s$ . Specifically, a 2D global average pooling operation is applied to  $v$  along the spatial dimensions, followed by a projection layer to obtain the global features  $v_g$ . The sequential tokens  $v_s$  are derived by flattening  $v$  along the spatial dimension and processing it through the same projection layer. The projection layer (Proj) is a linear layer without any activation function, serves as an interface between the visual and linguistic modalities by mapping visual features to a dimensionality  $E$  that aligns with

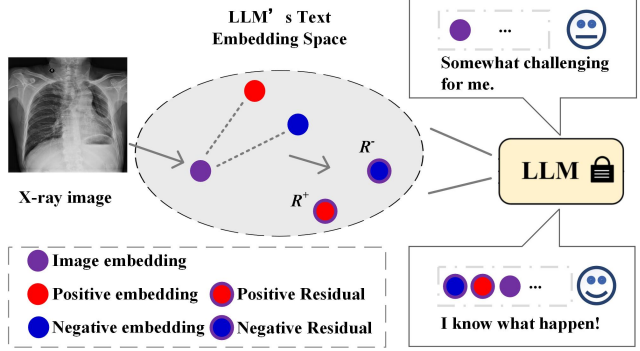


Figure 3. By concatenating the residual information with the current X-ray image as input prompt, the LLM leverages its intrinsic in-context learning capabilities to better understand the variations and generate more accurate medical reports.

the token embedding size of the language model. This operation yields global features  $v_g \in \mathbb{R}^E$  and sequential tokens  $v_s \in \mathbb{R}^{L \times E}$ , both of which are compatible with the language model’s processing requirements. Mathematically speaking,

$$v_g = Proj(avgPool2D(v)), \quad (5)$$

$$v_s = Proj(Flatten(v)), \quad (6)$$

Here,  $v_g$  captures the global information of the X-ray image, while the sequential tokens  $v_s$  represent local visual features. In our framework,  $v_g$  is employed for residual computations due to its capacity to preserve compact yet comprehensive global representations.

#### 3.3.2 Context Sample Retrieval

Given the visual tokens of the input X-ray images, one can directly feed them into the large language model to generate the medical reports, clearly, this approach will still reach its performance bottleneck. The context learning methods [12, 51] suggest that other samples in the training set may still play a positive role in each round of model optimization. Therefore, we consider designing a method to mine samples that are positively and negatively correlated with the current sample to enhance discriminative feature learning, thereby better guiding the LLM to generate accurate medical reports.

• **Positive and Negative Sample Selection.** For each sample in a mini-batch, we can retrieve its context samples based on keywords in the medical reports. In our implementation, we exploit two different approaches: 1). We adopt the CheXbert [42] to find the possible 14 kinds of diseases from the annotated medical report. If the sample is annotated as *No Finding*, we treat it as a negative context sample (without disease), otherwise positive (with disease).

2). We observe that radiologists tend to emphasize significant findings in X-ray images by including the word *Note* in their reports, making such images suitable for clear differentiation than other X-ray images in our sample selection process. To support our hypothesis, as illustrated in Fig. 1 (e), we used t-SNE to map the image features into a lower-dimensional space, and the results show a clear distinction between images associated with reports containing the word *Note* and those without it. Accordingly, we classify context samples containing the word *Note* as positive samples and those without it as negative samples, and then perform random sampling separately within each group.

After retrieving the context samples, we extract global visual features from the X-ray images using the same procedure as in Eq. 5. To distinguish these from the current training sample’s feature  $v_g$ , we denote the context features as  $\{c_{g,1}, c_{g,2}, \dots, c_{g,n}\}$ , where each  $c_{g,i} \in \mathbb{R}^E$  represents the  $E$ -dimensional embedding of the  $i$ -th context sample.

• **Residual Calculation.** To guide the large language model to generate more accurate medical reports, we measure the difference between the current input X-ray sample and context samples, and term the difference as *residual tokens*. For each context sample, we assign a disease prompt *With disease* or *Normal* and also take the visual-prompt difference into consideration. All quantities below are *token embeddings* in the same projected language space  $\mathbb{R}^E$ . The residual tokens are calculated as follows:

$$R_{v,i}^+ = v_g - c_{g,i}^+, \quad R_{v,i}^- = v_g - c_{g,i}^-, \quad (7)$$

$$R_t^+ = [v_g - t_1^+, v_g - t_2^+, \dots, v_g - t_p^+], \quad (8)$$

$$R_t^- = [v_g - t_1^-, v_g - t_2^-, \dots, v_g - t_p^-], \quad (9)$$

In the above equations,  $R_{v,i}^+$  and  $R_{v,i}^-$  denote the residual tokens of the  $i$ -th positive and negative image, while  $R_t^+$  and  $R_t^-$  correspond to the residual tokens for the disease prompts. The notation  $[\cdot, \cdot]$  indicates the concatenation operation.

To ensure the validity of directly subtracting textual prompts from visual embeddings in the LLM’s language space, we note that the prompts *With disease* and *Normal* are semantically opposed. Empirically, their average cosine similarity in the projection space after training is only 0.0165, indicating that the two prompts occupy well-separated regions. Thus, the subtraction operation can be interpreted as contrasting the observed image against alternative diagnostic categories.

To further couple textual and visual discrepancies, we insert  $R_{v,i}$  into  $R_t$  to form:

$$R_i^+ = [v_g - t_1^+, v_g - t_2^+, \dots, R_{v,i}^+, \dots, v_g - t_p^+], \quad (10)$$

$$R_i^- = [v_g - t_1^-, v_g - t_2^-, \dots, R_{v,i}^-, \dots, v_g - t_p^-], \quad (11)$$

where  $R_i^+$  and  $R_i^-$  denote the residual tokens corresponding to the  $i$ -th positive and negative context sample.

Therefore, the final prompt for the LLM is constructed by orderly concatenating the residuals and tokenized features as follows:

$$\text{Prompt} = [R_1^-, R_1^+, R_2^-, R_2^+, \dots, R_n^+, R_n^+, v_s, T], \quad (12)$$

Here,  $T = \{t_1, t_2, \dots, t_k\}$  denotes the sequence of token embeddings obtained by processing the general instruction prompt with the LLM’s tokenizer. To leverage the LLM’s in-context learning ability, we prioritize residuals by placing them at the beginning of the prompt sequence.

As illustrated in Fig. 3, by capturing the semantic and visual discrepancies between the current image and the textual prompts, the residuals enable the LLM to better align visual and textual information. During the inference phase, the context sample pairs are selected from the training set, ensuring consistency with the training process.

### 3.3.3 LLM Head & Loss Function

The Large Language Model serves as the core component for generating comprehensive and precise medical reports from X-ray images. In our experiments, various LLMs are evaluated to achieve higher performance, including lightweight LLM Qwen1.5 (0.5B, 1.8B, 4B, 7B) [2], the medium-sized Llama2 (7B) [47], Llama3 (8B) [13], and large-scale MedicalGPT (13B) [58]. For even larger LLMs, considering the computational cost, this paper will not consider them for the time being.

To optimize our R2GenCSR framework, we adopt the cross-entropy loss function to measure the difference between the generated medical reports and the ground truth annotations. Specifically, we apply instruction-tuning to the LLM to generate medical reports, maintaining its original auto-regressive training objective. During this process, the LLM is fine-tuned specifically on the tokens of the medical report, guided by the instruction prompt that encapsulates the visual and textual residuals. Our loss function is defined as the negative log-likelihood of the sequence of report tokens. This can be formulated as:

$$\mathcal{L} = - \sum_{i=1}^L \log p_{\theta}(y_i | \text{Prompt}, Y_{r,<i}). \quad (13)$$

where  $\theta$  denotes the trainable parameters, and  $L$  is the length of the whole medical report.  $y_i$  is the token being predicted at the current step  $i$ , *Prompt* is the instruction prompt that includes the residuals and tokenized features, and  $Y_{r,<i}$  is the sequence of report tokens before the current prediction token  $y_i$ . The instruction-tuning ensures that the LLM generates a report that aligns with the provided instructions and context, thus producing a coherent and informative medical report.

Table 1. Comparison of our model’s performance on the IU X-Ray and MIMIC-CXR datasets. The symbol † indicates that we follow the R2Gen annotation using *Findings* and evaluate with our method because their report modifies the ground truth to an *Impression* concatenated with *Findings*. The best result is highlighted in bold, and the second-best result is underlined.

Dataset	Methods	Year	BLEU-1	BLEU-2	BLEU-3	BLEU-4	ROUGE-L	METEOR	CIDEr
IU X-Ray	R2Gen [7]	EMNLP 2020	0.470	0.304	0.219	0.165	0.371	0.187	-
	R2GenCMN [8]	ACL-IJCNLP 2021	0.475	0.309	0.222	0.170	0.375	0.191	-
	PPKD [29]	CVPR 2021	0.483	0.315	0.224	0.168	0.376	0.187	0.351
	AlignTrans [63]	MICCAI 2021	0.484	0.313	0.225	0.173	0.379	0.204	-
	Clinical-BERT [59]	AAAI 2022	0.495	0.330	0.231	0.170	0.376	0.209	0.432
	METransformer [55]	CVPR 2023	0.483	0.322	0.228	0.172	0.380	0.192	0.435
	DCL [26]	CVPR 2023	-	-	-	0.163	0.383	0.193	<b>0.586</b>
	RAMT [65]	IEEE TMM 2023	0.482	0.310	0.221	0.165	0.377	0.195	-
	Token-Mixer [62]	IEEE TMI 2024	0.483	<u>0.338</u>	<u>0.250</u>	<u>0.190</u>	<b>0.402</b>	0.208	0.482
	PromptMRG [21]	AAAI 2024	0.401	-	-	0.098	0.160	<b>0.281</b>	-
	BootstrappingLLM [28]	AAAI 2024	<u>0.499</u>	0.323	0.238	0.184	0.390	0.208	-
	FMVP [34]	IEEE TMM 2024	0.485	0.315	0.225	0.169	0.398	0.201	-
	AHP-Full [64]	IEEE JBHI 2025	0.502	0.338	0.250	0.196	0.388	0.212	0.670
	R2GenGPT† [54]	Meta Radiology 2023	0.465	0.299	0.214	0.161	0.376	0.219	0.542
R2GenCSR	Ours	<b>0.514</b>	<b>0.351</b>	<b>0.262</b>	<b>0.206</b>	<u>0.401</u>	0.215	<u>0.579</u>	
MIMIC-CXR	R2Gen [7]	EMNLP 2020	0.353	0.218	0.145	0.103	0.277	0.142	-
	R2GenCMN [8]	ACL-IJCNLP 2021	0.353	0.218	0.148	0.106	0.278	0.142	-
	PPKD [29]	CVPR 2021	0.360	0.224	0.149	0.106	0.284	0.149	0.237
	AlignTrans [63]	MICCAI 2021	0.378	0.235	0.156	0.112	0.283	0.158	-
	Clinical-BERT [59]	AAAI 2022	0.383	0.230	0.151	0.106	0.275	0.144	0.151
	METransformer [55]	CVPR 2023	0.386	0.250	0.169	0.124	0.291	0.152	<b>0.362</b>
	DCL [26]	CVPR 2023	-	-	-	0.109	0.284	0.150	<u>0.281</u>
	RAMT [65]	IEEE TMM 2023	0.362	0.229	0.157	0.113	0.284	0.153	-
	Token-Mixer [62]	IEEE TMI 2024	<u>0.409</u>	0.257	0.175	0.124	0.288	0.158	0.163
	PromptMRG [21]	AAAI 2024	0.398	-	-	0.112	0.268	0.157	-
	BootstrappingLLM [28]	AAAI 2024	0.402	<u>0.262</u>	<u>0.180</u>	<u>0.128</u>	<u>0.291</u>	<b>0.175</b>	-
	FMVP [34]	IEEE TMM 2024	0.389	0.236	0.156	0.108	0.284	0.150	-
	AHP-Full [64]	IEEE JBHI 2025	0.400	0.250	0.172	0.126	0.285	0.154	0.169
	R2GenGPT† [54]	Meta Radiology 2023	0.408	0.256	0.174	0.125	0.285	0.167	0.244
R2GenCSR	Ours	<b>0.420</b>	<b>0.268</b>	<b>0.186</b>	<b>0.136</b>	<b>0.291</b>	<u>0.167</u>	0.267	

Table 2. Comparison on the CheXpert Plus dataset.

Method	Bleu-4	ROUGE-L	METEOR	CIDEr
R2Gen [7]	0.091	0.262	0.131	-
R2GenRL [39]	0.035	0.186	0.101	0.012
R2GenCMN [8]	0.095	0.262	0.142	-
R2Gen-GPT [54]	0.102	0.267	0.157	0.179
R2GenCSR	<b>0.103</b>	<b>0.272</b>	<b>0.163</b>	<b>0.193</b>

Table 3. Comparing the Clinical Efficacy (CE) metrics of different models on the Mimic-CXR dataset.

Method	Year	Precision	Recall	F1
R2Gen [7]	EMNLP 2020	0.333	0.273	0.276
METransformer [55]	CVPR 2023	0.364	0.309	0.311
KiUT [20]	CVPR 2023	0.371	0.318	0.321
R2GenGPT [54]	Meta Radiology 2023	0.392	<u>0.387</u>	<u>0.389</u>
RAMT [65]	IEEE TMM 2023	0.380	0.342	0.335
DCL [26]	CVPR 2023	<u>0.471</u>	0.352	0.373
MedRAT [16]	ECCV 2024	0.285	0.265	0.227
HERGen [50]	ECCV 2024	0.415	0.301	0.317
R2GenCSR	Ours	<b>0.551</b>	<b>0.432</b>	<b>0.484</b>

## 4. Experiment

### 4.1. Datasets and Evaluation Metrics

We evaluate the performance of our model on three datasets, including **IU X-Ray** [10], **MIMIC-CXR** [23], and **CheXpert Plus** [6] dataset. A brief introduction to these datasets is given below. For all datasets, we use only the "Findings" section as the ground truth for evaluation.

- **IU X-Ray** [10] is one of the most widely used publicly accessible medical image datasets in the field of medical report generation, which was released on year 2016. It contains 7,470 images and 3,955 radiology reports, each consisting of four parts: indication, comparison, *Findings*, and *Impression*. For a fair comparison, we have used the same dataset partition protocols as R2GenGPT and set the training/val/test for the dataset to 7:1:2.

- **MIMIC-CXR** [23] is a large publicly available dataset of chest radiographs with free-text radiology reports. These records, comprising 377, 110 radiographic images and 227, 835 radiology reports collected from 65, 379 individuals, span the years 2011-2016 and originate from the Beth Israel Deaconess Medical Center Emergency Department in Boston, MA. For a fair comparison, we used the same

dataset partition protocols as R2GenGPT, where 270,790 samples were used to train the model, and another 2,130 and 3,858 samples were used as validation and test sets, respectively.

- **CheXpert Plus** [6] is a large, newly released, organized med dataset with 223K radiology report-X-ray pairs from 64.7K patients, with each report detailed into 11 sections and X-rays in DICOM format with 47 metadata elements. It’s annotated for 14 chest conditions and patient metadata. We utilize the *Findings* as our ground truth and randomly partition the dataset into a ratio of 7:1:2, which consists of training, validation, and testing sets with 40,463, 5,780, and 11,562 samples respectively. The split protocols for this dataset will be released for other researchers to reproduce our experiments.

For radiology report generation, we evaluate our model using four widely adopted natural language generation (NLG) metrics: CIDEr [49], BLEU [38], ROUGE-L [27], and METEOR [3]. Specifically, CIDEr measures the consensus between generated and reference reports by computing the cosine similarity of n-grams, emphasizing the semantic relevance of medical descriptions. BLEU evaluates the precision of n-grams (up to 4-grams) in generated reports compared to reference reports, ensuring the accuracy of key medical terms and phrases. ROUGE-L focuses on the longest common subsequences between generated and reference reports, assessing the recall of critical clinical information. METEOR incorporates precision, recall, stemming, and synonymy matching, providing a balanced evaluation of the alignment between generated and reference reports.

In addition to NLG metrics, we also evaluate clinical relevance in generated reports using Clinical Efficacy (CE) [31]. Following R2Gen [7] and DCL [26], we extract disease labels from reports using the CheXpert labeler and compute micro-averaged Precision, Recall, and F1 scores on the MIMIC-CXR dataset.

## 4.2. Implementation Details

In our experiments, the input X-ray image is default resized as  $224 \times 224$ , and the beam search is adopted for the report generation. The beam width is set as 5 and 3 for the IU X-Ray and MIMIC-CXR datasets, respectively. The number of positive/negative sample pairs is set to 3. The training procedure is conducted on a server with NVIDIA A800 80GB GPUs using a mixed precision. We train the proposed R2GenCSR model for 20 and 25 epochs on the MIMIC-CXR and IU X-Ray datasets, respectively. The mini-batch sizes are 36 and 32 for the MIMIC-CXR and IU X-Ray datasets, and both models are trained using a learning rate of  $1e-4$ . The CheXpert Plus dataset adopts the same training protocol as MIMIC-CXR. More details can be found in our source code.

## 4.3. Comparison on Public Benchmarks

- **Results on IU X-Ray dataset.** As shown in Table 1, we compare our results to state-of-the-art (SOTA) methods on the IU X-Ray datasets. It is important to note that the R2GenGPT method’s reported results were based on a concatenation of *Impression* and *Findings* as the testing ground truth, which we believe is not representative of general scenarios so we re-trained their method using only with *Findings*. Our method demonstrates competitive performance, achieving a BLEU-4 score of 0.206, which surpasses existing methods, highlighting the effectiveness of our context-guided efficient radiology report generation framework.

- **Results on MIMIC-CXR dataset.** As shown in Table 1, we report our results on the large-scale MIMIC-CXR dataset. Our method achieved a BLEU-1 score of 0.420, a BLEU-4 score of 0.136, and a ROUGE-L score of 0.291, indicating its ability to generate precise and contextually relevant medical reports. The CIDEr score of 0.267 suggests that the method produces descriptive reports that closely match the reference summaries, highlighting its practical application in clinical settings. Note that our approach employs a dataset-specific strategy, utilizing Llama2 as the text decoder, which is the model variant optimized for the MIMIC-CXR dataset, ensuring that the model is well-suited to the medical reports it processes. Notably, as illustrated in Table 3, our method achieves competitive CE scores for the MIMIC-CXR dataset, highlighting the robustness of our model in handling imbalanced datasets by effectively capturing relationships in both major and minor categories.

- **Results on CheXpert Plus dataset.** As shown in Table 2, we re-train R2Gen series medical report generation models on the recently released CheXpert Plus dataset, including R2Gen [7], R2GenRL [39], R2GenCMN [8], and R2Gen-GPT [54]. The Llama2-based R2Gen-GPT outperforms others on all four metrics, but our proposed R2GenCSR model further surpasses R2Gen-GPT, achieving improvements of 0.001, 0.005, 0.006, and 0.014 on Bleu-4, ROUGE-L, METEOR, and CIDEr, respectively. These results validate the effectiveness of our proposed modules for radiology report generation.

- **Results on GREEN Metrics.** Inspired by Liu et al. [32] and GREEN [37], GREEN evaluates factual correctness through explicit error-type matching, achieving close alignment with expert judgment. Since the GREEN metric was introduced recently and has not been widely adopted in earlier studies, we compare a limited set of methods. We follow exactly the notation and summation format used in the original GREEN formulation. The GREEN score in the original formulation is defined as:

$$\text{GREEN} = \frac{\# \text{ matched findings}}{\# \text{ matched findings} + \sum_{i=(a)}^{(f)} \# \text{ error}_{\text{sig},i}} \quad (14)$$

Table 4. Component analysis of the key modules in our framework on MIMIC-CXR and IU X-Ray dataset. **B-1**, **B-4**, **R-L**, and **M** is short for BIEU-1, BIEU-4, ROUGE-L, METEOR, respectively. **P**, **R**, and **F1** is short for Precision, Recall, F1 score, respectively.

Index	VMamba	Context	Fixed pair	Qwen1.5	Llama2	MIMIC-CXR							IU X-Ray				
						NLG Metrics				Clinical Efficacy			GREEN	NLG Metrics			
						B-1	B-4	R-L	M	P	R	F1		B-1	B-4	R-L	M
#1	✗	✗	✗	✗	✓	0.407	0.126	0.282	0.162	0.519	0.400	0.452	0.316	0.454	0.173	0.376	0.210
#2	✓	✗	✗	✗	✓	0.415	0.127	0.285	0.165	0.552	0.430	0.483	0.325	0.476	0.175	0.377	0.209
#3	✓	✓	✗	✗	✓	0.416	0.131	0.289	0.167	0.544	0.423	0.476	0.327	0.496	0.176	0.387	0.209
#4	✓	✓	✓	✗	✓	<b>0.420</b>	<b>0.136</b>	<b>0.291</b>	<b>0.167</b>	<b>0.551</b>	<b>0.432</b>	<b>0.484</b>	<b>0.329</b>	0.483	0.180	0.385	0.219
#5	✗	✗	✗	✓	✗	0.327	0.110	0.282	0.140	0.536	0.354	0.426	0.298	0.478	0.180	0.384	0.195
#6	✓	✗	✗	✓	✗	0.348	0.114	0.282	0.144	0.526	0.361	0.428	0.297	0.498	0.189	0.387	0.203
#7	✓	✓	✗	✓	✗	0.312	0.105	0.283	0.138	0.551	0.366	0.440	0.296	0.503	0.195	0.389	0.214
#8	✓	✓	✓	✓	✗	0.359	0.116	0.283	0.146	0.523	0.373	0.436	0.305	<b>0.514</b>	<b>0.206</b>	<b>0.401</b>	<b>0.215</b>

Table 5. **GREEN Metrics** of R2GenCSR. Clinically Significant Errors denote (a) False report of a finding in the candidate, (b) Missing a finding present in the reference, (c) Misidentification of a finding’s anatomic location/position, (d) Misassessment of the severity of a finding, (e) Mentioning a comparison that isn’t in the reference, (f) Omitting a comparison detailing a change from a prior study. Metrics with  $\uparrow$  indicating higher is better and  $\downarrow$  indicating lower is better.

Dataset	Method	Clinically Significant Errors $\downarrow$						$\sum_{i=(a)}^{(f)}$ # error <sub>sig.,i</sub> $\downarrow$	# matched findings $\uparrow$	GREEN $\uparrow$
		(a)	(b)	(c)	(d)	(e)	(f)			
MIMIC-CXR	R2Gen [7]	1.310	3.089	<b>0.103</b>	<b>0.201</b>	0.082	0.142	4.926	1.803	0.283
	R2GenCMN [8]	1.383	2.963	0.127	0.228	<b>0.081</b>	0.161	4.942	1.935	0.297
	CvT2DistilGPT2 [36]	<b>1.150</b>	2.881	0.146	0.234	0.103	0.153	4.666	1.967	0.313
	R2GenGPT [54]	1.636	<b>2.206</b>	0.154	0.283	0.149	<b>0.085</b>	<b>4.513</b>	2.059	0.326
	R2GenCSR	1.577	2.256	0.156	0.311	0.144	0.098	4.541	<b>2.099</b>	<b>0.329</b>
CheXpert Plus	R2Gen [7]	<b>1.235</b>	3.638	<b>0.150</b>	<b>0.122</b>	<b>0.021</b>	0.103	5.269	0.938	0.168
	R2GenCMN [8]	1.512	3.336	0.218	0.165	0.043	0.126	5.399	1.179	0.197
	CvT2DistilGPT2 [36]	1.815	3.289	0.252	0.182	0.091	0.132	5.760	1.166	0.185
	R2GenGPT [54]	1.928	2.361	0.280	0.262	0.108	<b>0.059</b>	<b>4.998</b>	1.521	0.244
	R2GenCSR	2.015	<b>2.311</b>	0.258	0.251	0.121	0.069	5.024	<b>1.535</b>	<b>0.246</b>

Here, the subcategory labels (a)–(f) are the six predefined error types introduced in [37], corresponding to (a) false report of a finding; (b) missing a reference finding; (c) incorrect identification of anatomical location; (d) misassessment of severity; (e) spurious comparison not present in the reference; (f) omission of a comparison describing change from a prior study.

As shown in Table 5, R2GenCSR attains the highest GREEN scores across the evaluated datasets. This improvement is primarily driven by an increased number of matched findings, which improves the matched-to-error ratio in Eq. (14). While our model does not uniformly achieve the lowest count for every individual clinically significant error subcategory, its larger set of correctly identified findings yields a more favorable balance between correct findings and errors compared with competing methods. Overall, our model better preserves clinically relevant findings while maintaining comparable levels of clinically significant errors, leading to improved factual reliability of the generated reports.

#### 4.4. Component Analysis

We conduct a detailed component analysis of our proposed framework on the IU X-Ray and MIMIC-CXR datasets to investigate the impact of each key module, in-

cluding VMamba, the use of contextual information, the fixed-pair strategy, and the choice of language model, as shown in Table 4. Specifically, replacing the Swin Transformer with VMamba yields richer visual representations and improved performance. The incorporation of contextual information facilitates the generation of higher-quality radiology reports, while the fixed-pair sampling strategy enhances metric scores by effectively leveraging both positive and negative samples.

Moreover, Qwen1.5 performs better than Llama2 on the IU X-Ray dataset. This can be explained by the scale-dependent behavior of large language models. Since IU X-Ray is relatively small, the smaller Qwen1.5 model is less sensitive to data sparsity and less prone to overfitting on limited patterns, allowing it to perform competitively or even better than larger models. When all components are present, consistent improvement is observed across multiple evaluation metrics, which indicates that the method generalizes across different language models. Based on these comprehensive experiments, our method is effective and robust in generating radiology reports.

#### 4.5. Ablation Study

In this section, we conduct a series of ablation studies to evaluate the impact of various components within our pro-

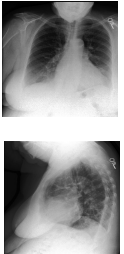
Image	Ground Truth	R2GenGPT	Ours
	Pa and lateral views of the chest provided. There is no focal consolidation effusion or pneumothorax. The cardiomeastinal silhouette is stable and top-normal in size. Imaged osseous structures are intact. No free air below the right hemidiaphragm is seen.	The lungs are clear without focal consolidation. No pleural effusion or pneumothorax is seen. The cardiac and mediastinal silhouettes are unremarkable. Atherosclerotic calcifications are noted at the aortic arch. Surgical clips are noted in the right upper quadrant of the abdomen compatible with prior cholecystectomy.	Pa and lateral views of the chest provided. There is no focal consolidation effusion or pneumothorax. The cardiomeastinal silhouette is normal. Imaged osseous structures are intact. No free air below the right hemidiaphragm is seen. Surgical clips project over the right upper quadrant. Mild degenerative changes are noted in the thoracic spine.
<i>Clinically Significant Errors</i>	<b>R2GenGPT:</b> Error (a) false finding: "atherosclerotic calcifications at aortic arch" not in GT. Error (a) false finding: "surgical clips ... prior cholecystectomy" not in GT. Error (b) missing finding: skips "lateral view provided" and "stable/top-normal size" of cardiomeastinal silhouette.	<b>Ours:</b> Error (a) false finding: "surgical clips" and "degenerative changes" not in GT. Error (d) severity misassessment: says "normal" instead of "stable and top-normal in size" → underestimates borderline size.	

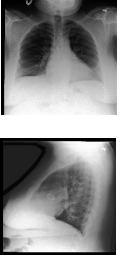
Image	Ground Truth	R2GenGPT	Ours
	Frontal and lateral views of the chest were obtained. The patient is status post median sternotomy and aortic valve replacement. There is minimal bibasilar atelectasis. No focal consolidation pleural effusion or pneumothorax is seen. Cardiac and mediastinal silhouettes are unremarkable.	Frontal and lateral views of the chest. The lungs are clear of focal consolidation or effusion. Cardiomeastinal silhouette is within normal limits. No acute osseous abnormality detected. Prosthetic aortic valve and mitral valve replacements are noted. Median sternotomy wires are intact. Clips in the right upper quadrant of the abdomen are unchanged.	Frontal and lateral views of the chest were obtained. The patient is status post median sternotomy and aortic valve replacement. There is no focal consolidation pleural effusion or evidence of pneumothorax. The cardiac and mediastinal silhouettes are unremarkable. Bony structures are intact. No free air below the right hemidiaphragm is seen.
<i>Clinically Significant Errors</i>	<b>R2GenGPT:</b> Error (a) false finding: "prosthetic mitral valve replacement" not in GT (GT only has AVR). Error (a) false finding: "clips in right upper quadrant of abdomen" not in GT. Error (b) missing finding: skips "minimal bibasilar atelectasis".	<b>Ours:</b> Error (a) false finding: "bony structures intact" and "no free air below right hemidiaphragm" not in GT. Error (b) missing finding: skips "minimal bibasilar atelectasis".	

Figure 4. Comparison of X-ray images with corresponding ground truth reports and generated reports from R2GenGPT and our model on the MIMIC-CXR dataset. Sentences with semantically mismatched content are highlighted in red, while semantically matched sentences are highlighted in yellow. Clinically Significant Errors following the GREEN [37]: (a) False report of a finding in the candidate, (b) Missing a finding present in the reference, (c) Misidentification of a finding’s anatomic location/position, (d) Misassessment of the severity of a finding, (e) Mentioning a comparison that isn’t in the reference, (f) Omitting a comparison detailing a change from a prior study.

Table 6. Results of different VMamba model scales on the IU X-Ray dataset.

Method	Bleu-1	Bleu-4	ROUGE-L	METEOR
<b>Tiny</b>	0.484	0.196	0.398	0.205
<b>Small</b>	0.505	0.204	0.391	0.212
<b>Base</b>	0.514	0.206	0.401	0.215

Table 7. Results of different context retrieve methods on IU X-Ray.

Method	Bleu-1	Bleu-4	ROUGE-L	METEOR
<b>Chexbert</b>	0.495	0.195	0.391	0.207
<b>Random</b>	0.504 ± 0.004	0.197 ± 0.002	0.390 ± 0.002	0.213 ± 0.004
<b>Keyword</b>	0.514	0.206	0.401	0.215

posed context-guided efficient radiology report generation framework. While IU X-Ray serves as the primary dataset for detailed component analysis due to its suitability for iterative validation, we additionally include key ablation experiments on the MIMIC-CXR dataset to confirm the consistency and generalizability of our findings.

- **Analysis of different VMamba backbones.** As shown

Table 8. Ablation of context samples on IU X-Ray dataset.

#Pairs	Bleu-1	Bleu-4	ROUGE-L	METEOR
<b>1</b>	0.513	0.196	0.390	0.215
<b>3</b>	0.514	0.206	0.401	0.215
<b>5</b>	0.490	0.182	0.375	0.203
<b>10</b>	0.491	0.182	0.383	0.205

in Table 6, we evaluate the Tiny, Small, and Base versions of VMamba on the IU X-Ray dataset. As the scale of the VMamba backbone increases, the performance metrics show a consistent improvement. The Base version of VMamba demonstrates the best overall performance, with improvements over the Small version of 0.009, 0.002, 0.010, and 0.003 in Bleu-1, Bleu-4, ROUGE-L, and METEOR, respectively. It confirms that a larger VMamba backbone can capture more intricate visual features from X-ray images, thereby enhancing the quality of the generated medical reports.

- **Analysis of different context sample retrieve methods.** As shown in Table 7, we assess the performance of three distinct methods: Chexbert [42] is utilized to ex-

Table 9. Feature subtraction at different stages on the IU X-Ray dataset. ‘Before-proj. VR’ denotes the visual residual conducted before projection, ‘After-proj. VR’ denotes the visual residual conducted after projection, and ‘After-proj. VR + TR’ denotes the visual and context-instructed text residuals conducted after projection.

Method	Bleu-1	Bleu-4	ROUGE-L	METEOR
Before-proj. VR	0.503	0.196	0.390	0.211
After-proj. VR	0.506	0.200	0.392	0.213
After-proj. VR + TR	0.514	0.206	0.401	0.215

tract 14 medical observations, we define the images corresponding to reports labeled “No Finding” serving as negative samples, while all other images are classified as positive. Despite its moderate performance, Chexbert provides a baseline for comparison. The Random method retrieves context samples in a completely random manner, without any division into positive or negative groups, and it leads to a slight improvement in the generation results. To ensure fairness and avoid accidental bias, we report its performance as mean  $\pm$  standard deviation over multiple runs with six randomly selected samples. The Keyword method retrieves samples based on the presence or absence of the word “Note” in the reports, as analyzed in the “Positive and Negative Sample Selection” subsection.

- **Analysis of the different number of context samples.** The Table 8 illustrates the performance across different numbers of context sample pairs. The results reveal an optimal point at 3 context sample pairs, which achieves higher scores than 10 pairs, with improvements for Bleu-1, Bleu-4, ROUGE-L, and METEOR of 0.023, 0.024, 0.018, and 0.010, respectively. As the number of context samples increases (from 3 to 10), there is a noticeable decline in performance across all metrics. We suggest that while additional context samples can contribute to a richer feature representation, an excessive number may introduce noise, detracting from the model’s ability to generate accurate and coherent reports. The use of a single context sample pair also yields competitive results, but the slight improvement seen with three pairs indicates that a moderate amount of context can enhance the learning process.

- **Analysis of different stages for feature subtraction.** As illustrated in Table 9, conducting visual subtraction in the large language model embedding space yields better results than subtraction outside of it, and when both visual and context-instructed text residuals are considered, all evaluation metrics show improvements after the LLM projection space, highlighting the importance of feature subtraction at different stages and confirming the effectiveness of the proposed approach in enhancing feature representation.

- **Analysis of different resolutions for report generation.** As shown in Table 10, we conducted experiments

Table 10. Results under different resolutions on IU X-Ray dataset.

Scale	Bleu-1	Bleu-4	ROUGE-L	METEOR
$512 \times 512$	0.500	0.196	0.388	0.205
$448 \times 448$	0.503	0.201	0.385	0.209
$224 \times 224$	0.514	0.206	0.401	0.215

Table 11. Evaluation between VMamba and Swin Transformer on MIMIC-CXR dataset.

Scale and Efficiency	R2GenCSR-VMamba	R2GenCSR-SwinT
Trainable Parameter	91.7 M	90.9 M
FLOPs	1852.35 G	1855.02 G
Training Time	3.98 h/Epoch	5.85 h/Epoch
Testing Time	0.52 h	0.52 h
Memory	75723 MB	70203 MB

on the IU X-Ray dataset using three image resolutions:  $512 \times 512$ ,  $448 \times 448$ , and  $224 \times 224$ . The performance metrics, including Bleu-1, Bleu-4, ROUGE-L, and METEOR, improved by 0.014, 0.010, 0.013 and 0.010 as the resolution decreased from  $512 \times 512$  to  $224 \times 224$ , respectively. This unexpected trend can be partially explained by the fact that we utilized the Vmamba model which was pre-trained on  $224 \times 224$  resolution and it is adept at processing and extracting meaningful features from images of this specific resolution.

- **Analysis of Positive vs. Negative Samples.** As shown in Table 12, using only positive samples or only negative samples already brings clear improvements over the baseline without residual guidance, confirming that each component individually contributes to enhancing report generation. Positive samples improve clinical efficacy metrics, while negative samples slightly improve GREEN score. Importantly, combining both positive and negative samples yields the best overall performance across all metrics, indicating their complementary effects in guiding the LLM to generate more accurate and comprehensive reports.

- **Analysis of Positive-Negative context-instructed text and Instruction prompt.** As shown in Table 13, we examine the influence of positive-negative context-instructed text and different instruction prompts on our model’s report generation quality. For instance, by modifying the context-instructed text from *Note: <Img>R<sub>v</sub><sup>-</sup></Img> normal. Note: <Img>R<sub>v</sub><sup>+</sup></Img> with disease. to Observation: <Img>R<sub>v</sub><sup>-</sup></Img> appears to be normal and healthy. Observation: <Img>R<sub>v</sub><sup>+</sup></Img> shows clear signs of disease.*, the Bleu-4 score decreased by 0.010. Similarly, by changing the instruction prompt from *Generate a comprehensive and detailed diagnosis report for this chest x-ray image. to Construct a full and methodical diagnostic summary for the chest X-ray displayed.*, the Bleu-4 score decreased by 0.007. These minor variations stem from the

Table 12. Ablation study using only positive or only negative samples on MIMIC-CXR and IU X-Ray. **Pos.** denotes positive samples, and **Neg.** denotes negative samples.

Pos.	Neg.	MIMIC-CXR							IU X-Ray				
		NLG Metrics				Clinical Efficacy			GREEN	NLG Metrics			
		B-1	B-4	R-L	M	P	R	F1		B-1	B-4	R-L	M
✗	✗	0.407	0.126	0.282	0.162	0.519	0.400	0.452	0.316	0.498	0.189	0.387	0.203
✓	✗	0.417	0.133	0.288	0.167	0.546	0.426	0.479	0.328	0.485	0.195	0.380	0.203
✗	✓	0.415	0.133	0.287	0.167	0.539	0.435	0.481	0.331	0.505	0.190	0.372	0.207
✓	✓	0.420	0.136	0.291	0.167	0.551	0.432	0.484	0.329	0.514	0.206	0.401	0.215

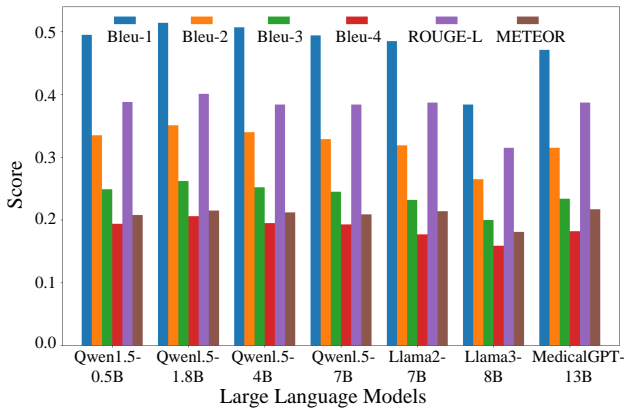


Figure 5. Performance comparison of LLMs on the IU X-Ray dataset, revealing significant variations across models with the Qwen series demonstrating superior performance on average.

LLM’s sensitivity to prompt wording. Concise and medically conventional phrasing aligns better with its pretrained medical language distribution. Although the differences in performance between the prompts are relatively small, optimizing prompts can subtly affect the model’s output.

• **Analysis of different LLMs for report generation.** As illustrated in Fig. 5, we present the performance among models of varying sizes and architectures, including the Qwen and Llama series models. The Qwen series models demonstrate superior performance on average, outperforming other models across multiple evaluation metrics. Specifically, the Qwen1.5-1.8B model demonstrates a notable improvement in metrics such as Bleu-4 and ROUGE-L by 0.206 and 0.401, respectively. However, the Llama3-8B model, despite its larger size, underperforms compared to the Qwen1.5-4B model, even worse than Llama2-7B on IU X-Ray dataset. The specialized MedicalGPT (Llama-13B) model exhibits competitive performance within the Llama series, showcasing the potential benefits of domain-specific fine-tuning for large language models in medical report generation tasks. Therefore, selecting an appropriate LLM that balances size, architecture, and domain spe-

cialization is necessary for optimal report generation performance.

• **Analysis of VMamba and Swin-Transformer for report generation.** In Table 11, we compare VMamba and Swin Transformer as vision backbones on a single A800 80G GPU. While R2GenCSR-VMamba has slightly more trainable parameters (91.7 M vs. 90.9 M) and higher memory usage (75,723 MB vs. 70,203 MB), it reduces training time per epoch from 5.85 hours to 3.98 hours. The FLOPs of VMamba are comparable to Swin Transformer (1852.35 G vs. 1855.02 G), and testing times are similar for both models. These results indicate that, despite the modest increase in memory usage, VMamba provides better training efficiency and accuracy trade-off for R2GenCSR.

• **Analysis of Backbone and Decoder Variants.** As shown in Table 14, we follow R2Gen [7] and R2GenMamba [44] by using a lightweight 3-layer, 8-head Transformer decoder instead of a large LLM. This setting provides a fair comparison to earlier baselines and isolates the effect of different visual encoders. We observe that replacing the Swin Transformer with VMamba yields consistent improvements, demonstrating that VMamba contributes to efficiency and accuracy even without relying on a large LLM. Moreover, when paired with a strong LLM (e.g., Qwen1.5-1.8B), our framework achieves further gains, indicating that while the LLM plays a dominant role in language fluency, our proposed retrieval and residual mechanisms contribute complementary benefits beyond backbone strength.

#### 4.6. Visualization

• **X-ray Medical Report.** Fig. 4 illustrates a side-by-side comparison of X-ray images alongside their respective ground truths and the reports generated by the baseline R2GenGPT model and our model. It is clear that our method is capable of producing reports that closely align with the ground truth, with only minor discrepancies highlighted in mismatching terms but the overall performance of our framework on the MIMIC-CXR dataset is promising.

• **Token-wise Attention Distribution.** Fig. 6 quantifies the attention scores allocated to each token position, with

Table 13. Analysis of prompt design variants on IU X-Ray. For interpretability, we replace text residuals  $R_t^-$ ,  $R_t^+$  and general instruction prompt  $T$  with their original text descriptions.

Method	Bleu-1	Bleu-4	ROUGE-L	METEOR
Note: $\langle \text{Img} \rangle R_v^- \langle / \text{Img} \rangle$ normal. Note: $\langle \text{Img} \rangle R_v^+ \langle / \text{Img} \rangle$ with disease. Human: $\langle \text{Img} \rangle v_s \langle / \text{Img} \rangle$ Generate a comprehensive and detailed diagnosis report for this chest xray image. $\backslash \text{nAssistant}$ :	0.514	0.206	0.401	0.215
Observation: $\langle \text{Img} \rangle R_v^- \langle / \text{Img} \rangle$ appears to be normal and healthy. Observation: $\langle \text{Img} \rangle R_v^+ \langle / \text{Img} \rangle$ shows clear signs of disease. Human: $\langle \text{Img} \rangle v_s \langle / \text{Img} \rangle$ Generate a comprehensive and detailed diagnosis report for this chest x-ray image. $\backslash \text{nAssistant}$ :	0.503	0.196	0.384	0.209
Indication: $\langle \text{Img} \rangle R_v^- \langle / \text{Img} \rangle$ shows no signs of pathology. Indication: $\langle \text{Img} \rangle R_v^+ \langle / \text{Img} \rangle$ exhibits symptoms of a medical condition. Human: $\langle \text{Img} \rangle v_s \langle / \text{Img} \rangle$ Generate a comprehensive and detailed diagnosis report for this chest x-ray image. $\backslash \text{nAssistant}$ :	0.502	0.200	0.393	0.211
Findings: $\langle \text{Img} \rangle R_v^- \langle / \text{Img} \rangle$ reveals a lack of abnormalities. Findings: $\langle \text{Img} \rangle R_v^+ \langle / \text{Img} \rangle$ reveals the presence of a pathology. Human: $\langle \text{Img} \rangle v_s \langle / \text{Img} \rangle$ Generate a comprehensive and detailed diagnosis report for this chest x-ray image. $\backslash \text{nAssistant}$ :	0.499	0.202	0.393	0.207
Note: $\langle \text{Img} \rangle R_v^- \langle / \text{Img} \rangle$ normal. Note: $\langle \text{Img} \rangle R_v^+ \langle / \text{Img} \rangle$ with disease. Human: $\langle \text{Img} \rangle v_s \langle / \text{Img} \rangle$ Construct a full and methodical diagnostic summary for the chest X-ray displayed. $\backslash \text{nAssistant}$ :	0.497	0.199	0.392	0.209
Note: $\langle \text{Img} \rangle R_v^- \langle / \text{Img} \rangle$ normal. Note: $\langle \text{Img} \rangle R_v^+ \langle / \text{Img} \rangle$ with disease. Human: $\langle \text{Img} \rangle v_s \langle / \text{Img} \rangle$ Develop a detailed and professional medical assessment from this chest X-ray image. $\backslash \text{nAssistant}$ :	0.504	0.196	0.393	0.217
Note: $\langle \text{Img} \rangle R_v^- \langle / \text{Img} \rangle$ normal. Note: $\langle \text{Img} \rangle R_v^+ \langle / \text{Img} \rangle$ with disease. Human: $\langle \text{Img} \rangle v_s \langle / \text{Img} \rangle$ Analyze and generate a detailed report on the findings of this chest X-ray. $\backslash \text{nAssistant}$ :	0.502	0.203	0.388	0.213

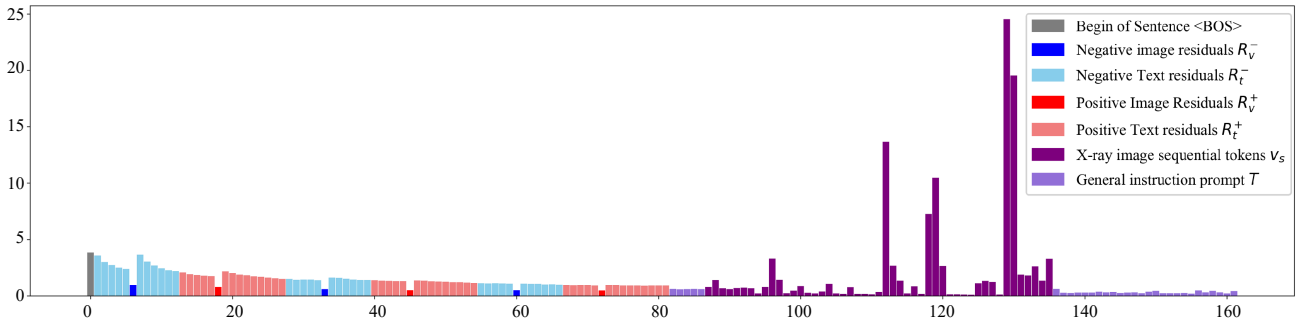


Figure 6. Distribution of aggregated attention weights in the LLM’s attention mechanism across token positions for an input X-ray image. Attention scores were computed via column-wise summation across the attention matrix. The x-axis denotes token position indices, while the y-axis represents the computed attention scores. The bar plot demonstrates the predominant influence of image sequential tokens  $v_s$ , with secondary contributions from negative residuals  $R^-$  and positive residuals  $R^+$ .

token types differentiated by color according to the legend. The scores are derived through column-wise aggregation of attention weights for a given X-ray image from the MIMIC-CXR dataset. Sequential image tokens ( $v_s$ , purple) receive the highest attention scores, indicating their primary role as carriers of diagnostic information. Notably, residual tokens attract significantly stronger attention compared to general

instruction prompt ( $T$ , medium purple), indicating that the LLM prioritizes these residual contextual prompts during report generation.

• **Feature Maps.** The X-ray image and its corresponding feature map are displayed side by side in Fig. 7. It is evident from the feature map that the VMamba vision backbone effectively extracts discriminative visual features from the X-

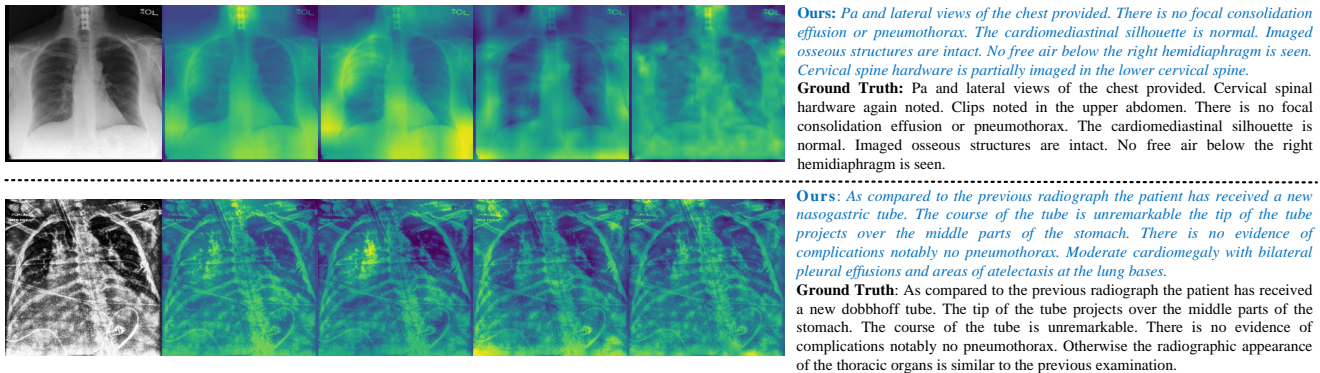


Figure 7. Visualization of the input X-ray image, intermediate feature maps from the Vmamba model blocks, and the generated radiology report on the MIMIC-CXR dataset.

Table 14. Analysis of backbone and decoder variants. "Transf." denotes a 3-layer, 8-head Transformer used as the language decoder.

Method	Bleu-1	Bleu-4	ROUGE-L	METEOR
R2Gen	0.470	0.165	0.371	0.187
R2Gen-Mamba	0.482	0.176	0.382	0.208
Vmamba + Transf.	0.493	0.176	0.377	0.198
Swin + Transf.	0.487	0.167	0.377	0.195
Vmamba + LLM	0.514	0.206	0.401	0.215

ray image, emphasizing regions of interest such as lesions, organs, and other anomalies. These extracted features supply detailed information for subsequent processing.

#### 4.7. Limitation Analysis

Although our proposed R2GenCSR achieves better performance on three large-scale report generation benchmark datasets, however, our model may still be limited by the following issues: 1). We adopt a simple retrieval strategy for context sample mining, more advanced retrieval techniques can be exploited to achieve better performance; 2). The knowledge about the disease is ignored in our R2GenCSR framework, this information may be useful to guide the X-ray image report generation task. In our future works, we will consider improving the proposed framework from the aforementioned two aspects.

### 5. Conclusion

In this paper, we have developed a novel context-guided efficient radiology report generation framework with the aim of enhancing the performance of Large Language Models in clinical settings. We introduced the Mamba model as a linear complexity vision backbone to effectively extract visual features from X-ray images, ensuring that the computational burden is significantly reduced while maintaining performance parity with the robust Transformer architecture.

Our approach was complemented by the integration of vision tokens, context information, and prompt statements to facilitate the generation of high-quality medical reports by the LLM. The proposed framework, extensively evaluated on the IU X-Ray, MIMIC-CXR, and CheXpert Plus datasets, has demonstrated its efficacy and state-of-the-art performance. Our work not only contributes to the advancement of automated medical report generation but also provides valuable insights for leveraging LLMs in other domains.

### Acknowledgement

This work was supported by the National Natural Science Foundation of China under Grant 62102205. Anhui Provincial Natural Science Foundation-Outstanding Youth Project, 2408085Y032. The authors acknowledge the High-performance Computing Platform of Anhui University for providing computing resources.

### References

- [1] Rohan Anil, Andrew M. Dai, Orhan Firat, Melvin Johnson, and et al. Palm 2 technical report, 2023.
- [2] Jinze Bai, Shuai Bai, Yunfei Chu, and et al. Qwen technical report. *arXiv preprint arXiv:2309.16609*, 2023.
- [3] Satyanjee Banerjee and Alon Lavie. Meteor: An automatic metric for mt evaluation with improved correlation with human judgments. In *Proceedings of the acl workshop on intrinsic and extrinsic evaluation measures for machine translation and/or summarization*, pages 65–72, 2005.
- [4] Tom B. Brown, Benjamin Mann, Nick Ryder, Melanie Subbiah, Jared Kaplan, Prafulla Dhariwal, Arvind Neelakantan, Pranav Shyam, Girish Sastry, Amanda Askell, Sandhini Agarwal, Ariel Herbert-Voss, Gretchen Krueger, Tom Henighan, Rewon Child, Aditya Ramesh, Daniel M. Ziegler, Jeffrey Wu, Clemens Winter, Christopher Hesse, Mark Chen, Eric Sigler, Mateusz Litwin, Scott Gray, Benjamin Chess, Jack Clark, Christopher Berner, Sam McCandlish, Alec Rad-

- ford, Ilya Sutskever, and Dario Amodei. Language models are few-shot learners. 2020.
- [5] Yiming Cao, Lizhen Cui, Lei Zhang, Fuqiang Yu, Zhen Li, and Yonghui Xu. Mmtn: multi-modal memory transformer network for image-report consistent medical report generation. In *Proceedings of the AAAI Conference on Artificial Intelligence*, pages 277–285, 2023.
- [6] Pierre Chambon, Jean-Benoit Delbrouck, Thomas Sounack, Shih-Cheng Huang, Zhihong Chen, Maya Varma, Steven QH Truong, Chu The Chuong, and Curtis P Langlotz. Chexpert plus: Augmenting a large chest x-ray dataset with text radiology reports, patient demographics and additional image formats. *arXiv preprint arXiv:2405.19538*, 2024.
- [7] Zhihong Chen, Yan Song, Tsung-Hui Chang, and Xiang Wan. Generating radiology reports via memory-driven transformer. In *Proceedings of the 2020 Conference on Empirical Methods in Natural Language Processing (EMNLP)*, pages 1439–1449, 2020.
- [8] Zhihong Chen, Yaling Shen, Yan Song, and Xiang Wan. Cross-modal memory networks for radiology report generation. In *Proceedings of the 59th Annual Meeting of the Association for Computational Linguistics and the 11th International Joint Conference on Natural Language Processing (Volume 1: Long Papers)*, pages 5904–5914, Online, 2021. Association for Computational Linguistics.
- [9] Tri Dao and Albert Gu. Transformers are SSMs: Generalized models and efficient algorithms through structured state space duality. In *International Conference on Machine Learning (ICML)*, 2024.
- [10] Dina Demner-Fushman, Marc D Kohli, Marc B Rosenman, Sonya E Shooshan, Laritza Rodriguez, Sameer Antani, George R Thoma, and Clement J McDonald. Preparing a collection of radiology examinations for distribution and retrieval. *Journal of the American Medical Informatics Association*, 23(2):304–310, 2016.
- [11] Jacob Devlin, Ming-Wei Chang, Kenton Lee, and Kristina Toutanova. BERT: Pre-training of deep bidirectional transformers for language understanding. In *Proceedings of the 2019 Conference of the North American Chapter of the Association for Computational Linguistics: Human Language Technologies, Volume 1 (Long and Short Papers)*, pages 4171–4186, Minneapolis, Minnesota, 2019. Association for Computational Linguistics.
- [12] Qingxiu Dong, Lei Li, Damai Dai, Ce Zheng, Zhiyong Wu, Baobao Chang, Xu Sun, Jingjing Xu, and Zhifang Sui. A survey on in-context learning. *arXiv preprint arXiv:2301.00234*, 2022.
- [13] Abhimanyu Dubey, Abhinav Jauhri, Abhinav Pandey, Abhishek Kadian, Ahmad Al-Dahle, Aiesha Letman, Akhil Mathur, Alan Schelten, Amy Yang, Angela Fan, et al. The llama 3 herd of models. *arXiv preprint arXiv:2407.21783*, 2024.
- [14] Albert Gu and Tri Dao. Mamba: Linear-time sequence modeling with selective state spaces. *arXiv preprint arXiv:2312.00752*, 2023.
- [15] Albert Gu, Karan Goel, and Christopher Re. Efficiently modeling long sequences with structured state spaces. In *International Conference on Learning Representations*, 2022.
- [16] Elad Hirsch, Gefen Dawidowicz, and Ayellet Tal. Medrat: Unpaired medical report generation via auxiliary tasks. In *European Conference on Computer Vision*, pages 18–35. Springer, 2025.
- [17] Sepp Hochreiter and Jürgen Schmidhuber. Long short-term memory. *Neural Computation*, 9(8):1735–1780, 1997.
- [18] Daichi Horita, Naoto Inoue, Kotaro Kikuchi, Kota Yamaguchi, and Kiyoharu Aizawa. Retrieval-augmented layout transformer for content-aware layout generation. In *Proceedings of the IEEE/CVF Conference on Computer Vision and Pattern Recognition (CVPR)*, pages 67–76, 2024.
- [19] Lili Huang, Yiming Cao, Pengcheng Jia, Chenglong Li, Jin Tang, and Chuanfu Li. Knowledge-guided cross-modal alignment and progressive fusion for chest x-ray report generation. *IEEE Transactions on Multimedia*, pages 1–12, 2024.
- [20] Zhongzhen Huang, Xiaofan Zhang, and Shaoting Zhang. KiuT: Knowledge-injected u-transformer for radiology report generation. In *Proceedings of the IEEE/CVF Conference on Computer Vision and Pattern Recognition*, pages 19809–19818, 2023.
- [21] Haibo Jin, Haoxuan Che, Yi Lin, and Hao Chen. Promptmrg: Diagnosis-driven prompts for medical report generation. In *Proceedings of the AAAI Conference on Artificial Intelligence*, pages 2607–2615, 2024.
- [22] Baoyu Jing, Pengtao Xie, and Eric Xing. On the automatic generation of medical imaging reports. In *Proceedings of the 56th Annual Meeting of the Association for Computational Linguistics (Volume 1: Long Papers)*. Association for Computational Linguistics, 2018.
- [23] Alistair EW Johnson, Tom J Pollard, Seth J Berkowitz, Nathaniel R Greenbaum, Matthew P Lungren, Chih-ying Deng, Roger G Mark, and Steven Horng. Mimic-cxr, a de-identified publicly available database of chest radiographs with free-text reports. *Scientific data*, 6(1):317, 2019.
- [24] Jiaxuan Li, Duc Minh Vo, Akihiro Sugimoto, and Hideki Nakayama. Evcap: Retrieval-augmented image captioning with external visual-name memory for open-world comprehension. In *Proceedings of the IEEE/CVF Conference on Computer Vision and Pattern Recognition (CVPR)*, pages 13733–13742, 2024.
- [25] Kezhi Li, John Daniels, Chengyuan Liu, Pau Herrero, and Pantelis Georgiou. Convolutional recurrent neural networks for glucose prediction. *IEEE Journal of Biomedical and Health Informatics*, 24(2):603–613, 2020.
- [26] Mingjie Li, Bingqian Lin, Zicong Chen, Haokun Lin, Xiaodan Liang, and Xiaojun Chang. Dynamic graph enhanced contrastive learning for chest x-ray report generation. In *Proceedings of the IEEE/CVF Conference on Computer Vision and Pattern Recognition*, pages 3334–3343, 2023.
- [27] Chin-Yew Lin. Rouge: A package for automatic evaluation of summaries. In *Text summarization branches out*, pages 74–81, 2004.
- [28] Chang Liu, Yuanhe Tian, Weidong Chen, Yan Song, and Yongdong Zhang. Bootstrapping large language models for radiology report generation. In *Proceedings of the AAAI Conference on Artificial Intelligence*, pages 18635–18643, 2024.

- [29] Fenglin Liu, Xian Wu, Shen Ge, Wei Fan, and Yuexian Zou. Exploring and distilling posterior and prior knowledge for radiology report generation. In *Proceedings of the IEEE/CVF conference on computer vision and pattern recognition*, pages 13753–13762, 2021.
- [30] Fenglin Liu, Changchang Yin, Xian Wu, Shen Ge, Ping Zhang, and Xu Sun. Contrastive attention for automatic chest x-ray report generation. In *Findings of the Association for Computational Linguistics: ACL-IJCNLP 2021*, pages 269–280, 2021.
- [31] Guanxiong Liu, Tzu-Ming Harry Hsu, Matthew McDermott, Willie Boag, Wei-Hung Weng, Peter Szolovits, and Marzyeh Ghassemi. Clinically accurate chest x-ray report generation. In *Machine Learning for Healthcare Conference*, pages 249–269. PMLR, 2019.
- [32] Kang Liu, Zhuoqi Ma, Xiaolu Kang, Yunan Li, Kun Xie, Zhicheng Jiao, and Qiguang Miao. Enhanced contrastive learning with multi-view longitudinal data for chest x-ray report generation. *arXiv preprint arXiv:2502.20056*, 2025.
- [33] Yue Liu, Yunjie Tian, Yuzhong Zhao, Hongtian Yu, Lingxi Xie, Yaowei Wang, Qixiang Ye, and Yunfan Liu. Vmamba: Visual state space model. *arXiv preprint arXiv:2401.10166*, 2024.
- [34] Zhizhe Liu, Zhenfeng Zhu, Shuai Zheng, Yawei Zhao, Kunlun He, and Yao Zhao. From observation to concept: A flexible multi-view paradigm for medical report generation. *IEEE Transactions on Multimedia*, 26:5987–5995, 2024.
- [35] Feng Lu, Xiangyuan Lan, Lijun Zhang, Dongmei Jiang, Yaowei Wang, and Chun Yuan. Cricavpr: Cross-image correlation-aware representation learning for visual place recognition. In *Proceedings of the IEEE/CVF Conference on Computer Vision and Pattern Recognition (CVPR)*, pages 16772–16782, 2024.
- [36] Aaron Nicolson, Jason Dowling, and Bevan Koopman. Improving chest x-ray report generation by leveraging warm starting. *Artificial Intelligence in Medicine*, 144:102633, 2023.
- [37] Sophie Ostmeier, Justin Xu, Zhihong Chen, Maya Varma, et al. GREEN: Generative radiology report evaluation and error notation. In *Findings of the Association for Computational Linguistics: EMNLP 2024*, pages 374–390. Association for Computational Linguistics, 2024.
- [38] Kishore Papineni, Salim Roukos, Todd Ward, and Wei-Jing Zhu. Bleu: a method for automatic evaluation of machine translation. In *Proceedings of the 40th annual meeting of the Association for Computational Linguistics*, pages 311–318, 2002.
- [39] Han Qin and Yan Song. Reinforced cross-modal alignment for radiology report generation. In *Findings of the Association for Computational Linguistics: ACL 2022*, pages 448–458, Dublin, Ireland, 2022.
- [40] Alec Radford, Jeff Wu, Rewon Child, David Luan, Dario Amodei, and Ilya Sutskever. Language models are unsupervised multitask learners. 2019.
- [41] Karan Singhal, Tao Tu, Juraj Gottweis, Rory Sayres, Ellery Wulczyn, Mohamed Amin, Le Hou, Kevin Clark, Stephen R Pfohl, Heather Cole-Lewis, et al. Toward expert-level medical question answering with large language models, 2025.
- [42] Akshay Smit, Saahil Jain, Pranav Rajpurkar, Anuj Pareek, Andrew Y Ng, and Matthew Lungren. Combining automatic labelers and expert annotations for accurate radiology report labeling using bert. In *Proceedings of the 2020 Conference on Empirical Methods in Natural Language Processing (EMNLP)*, pages 1500–1519, 2020.
- [43] Jimmy T.H. Smith, Andrew Warrington, and Scott Linderman. Simplified state space layers for sequence modeling. In *The Eleventh International Conference on Learning Representations*, 2023.
- [44] Yongheng Sun, Yueh Z Lee, Genevieve A Woodard, Hongtu Zhu, Chunfeng Lian, and Mingxia Liu. R2gen-mamba: A selective state space model for radiology report generation. In *2025 IEEE 22nd International Symposium on Biomedical Imaging (ISBI)*, pages 1–4. IEEE, 2025.
- [45] Tim Tanida, Philip Müller, Georgios Kaissis, and Daniel Rueckert. Interactive and explainable region-guided radiology report generation. In *2023 IEEE/CVF Conference on Computer Vision and Pattern Recognition (CVPR)*. IEEE, 2023.
- [46] Hugo Touvron, Thibaut Lavril, Gautier Izacard, Xavier Martinet, Marie-Anne Lachaux, Timothée Lacroix, Baptiste Rozière, Naman Goyal, Eric Hambro, Faisal Azhar, Aurelien Rodriguez, Armand Joulin, Edouard Grave, and Guillaume Lample. Llama: Open and efficient foundation language models, 2023.
- [47] Hugo Touvron, Louis Martin, and et al. Llama 2: Open foundation and fine-tuned chat models, 2023.
- [48] Laurens Van der Maaten and Geoffrey Hinton. Visualizing data using t-sne. *Journal of machine learning research*, 9 (11), 2008.
- [49] Ramakrishna Vedantam, C Lawrence Zitnick, and Devi Parikh. Cider: Consensus-based image description evaluation. In *Proceedings of the IEEE conference on computer vision and pattern recognition*, pages 4566–4575, 2015.
- [50] Fuying Wang, Shenghui Du, and Lequan Yu. Hergen: Elevating radiology report generation with longitudinal data. In *Computer Vision–ECCV 2024: 19th European Conference*, 2024.
- [51] Xixi Wang, Bo Jiang, Xiao Wang, Jinhui Tang, and Bin Luo. Rethinking batch sample relationships for data representation: A batch-graph transformer based approach. *IEEE Transactions on Multimedia*, 26:1578–1588, 2024.
- [52] Xiao Wang, Yuehang Li, Wentao Wu, Jiandong Jin, Yao Rong, Bo Jiang, Chuanfu Li, and Jin Tang. Pre-training on high definition x-ray images: An experimental study. *arXiv preprint arXiv:2404.17926*, 2024.
- [53] Xiao Wang, Shiao Wang, Yuhe Ding, Yuehang Li, Wentao Wu, Yao Rong, Weizhe Kong, Ju Huang, Shihao Li, Haoxiang Yang, et al. State space model for new-generation network alternative to transformers: A survey. *arXiv preprint arXiv:2404.09516*, 2024.
- [54] Zhanyu Wang, Lingqiao Liu, Lei Wang, and Luping Zhou. R2genpt: Radiology report generation with frozen llms. *Meta-Radiology*, 1(3):100033, 2023.
- [55] Zhanyu Wang, Lingqiao Liu, Lei Wang, and Luping Zhou. Metransformer: Radiology report generation by transformer

- with multiple learnable expert tokens. In *Proceedings of the IEEE/CVF Conference on Computer Vision and Pattern Recognition (CVPR)*, pages 11558–11567, 2023.
- [56] Junde Wu, Jiayuan Zhu, and Yunli Qi. Medical graph rag: Towards safe medical large language model via graph retrieval-augmented generation. *arXiv preprint arXiv:2408.04187*, 2024.
- [57] Jilan Xu, Yifei Huang, Junlin Hou, Guo Chen, Yuejie Zhang, Rui Feng, and Weidi Xie. Retrieval-augmented egocentric video captioning. In *Proceedings of the IEEE/CVF Conference on Computer Vision and Pattern Recognition (CVPR)*, pages 13525–13536, 2024.
- [58] Ming Xu. Medicalgpt: Training medical gpt model. <https://github.com/shibing624/MedicalGPT>, 2023.
- [59] Bin Yan and Mingtao Pei. Clinical-bert: Vision-language pre-training for radiograph diagnosis and reports generation. In *Proceedings of the AAAI Conference on Artificial Intelligence*, pages 2982–2990, 2022.
- [60] Shi-Qi Yan, Jia-Chen Gu, Yun Zhu, and Zhen-Hua Ling. Corrective retrieval augmented generation, 2024.
- [61] Yan Yang, Jun Yu, Jian Zhang, Weidong Han, Hanliang Jiang, and Qingming Huang. Joint embedding of deep visual and semantic features for medical image report generation. *IEEE Transactions on Multimedia*, 25:167–178, 2021.
- [62] Yan Yang, Jun Yu, Zhenqi Fu, Ke Zhang, Ting Yu, Xianyun Wang, Hanliang Jiang, Junhui Lv, Qingming Huang, and Weidong Han. Token-mixer: Bind image and text in one embedding space for medical image reporting. *IEEE Transactions on Medical Imaging*, pages 1–1, 2024.
- [63] Di You, Fenglin Liu, Shen Ge, Xiaoxia Xie, Jing Zhang, and Xian Wu. Aligntransformer: Hierarchical alignment of visual regions and disease tags for medical report generation. In *Medical Image Computing and Computer Assisted Intervention–MICCAI 2021: 24th International Conference, Strasbourg, France, September 27–October 1, 2021, Proceedings, Part III 24*, pages 72–82. Springer, 2021.
- [64] Ting Yu, Wangwen Lu, Yan Yang, Weidong Han, Qingming Huang, Jun Yu, and Ke Zhang. Adapter-enhanced hierarchical cross-modal pre-training for lightweight medical report generation. *IEEE Journal of Biomedical and Health Informatics*, pages 1–15, 2025.
- [65] Ke Zhang, Hanliang Jiang, Jian Zhang, Qingming Huang, Jianping Fan, Jun Yu, and Weidong Han. Semi-supervised medical report generation via graph-guided hybrid feature consistency. *IEEE Transactions on Multimedia*, 26:904–915, 2024.
- [66] Ke Zhang, Yan Yang, Jun Yu, Hanliang Jiang, Jianping Fan, Qingming Huang, and Weidong Han. Multi-task paired masking with alignment modeling for medical vision-language pre-training. *IEEE Transactions on Multimedia*, 26:4706–4721, 2024.
- [67] Hong-Yu Zhou, Subathra Adithan, Julián Nicolás Acosta, Eric J. Topol, and Pranav Rajpurkar. A generalist learner for multifaceted medical image interpretation, 2024.
- [68] Lianghui Zhu, Bencheng Liao, Qian Zhang, Xinlong Wang, Wenyu Liu, and Xinggang Wang. Vision mamba: Efficient visual representation learning with bidirectional state space model. In *Forty-first International Conference on Machine Learning*, 2024.